Effect of lifter shape and operating parameters on the flow of materials in a pilot rotary kiln: Part III. Up-scaling considerations and segregation analysis

Alex Stéphane Bongo Njeng, Stéphane Vitu, Marc Clausse, Jean-Louis Dirion, Marie Debacq

Effect of lifter shape and operating parameters on the flow of materials in a pilot rotary kiln : Part III. Up-scaling considerations and segregation analysis

A.S. Bongo Njeng[a,b], S. Vitu[a], M. Clausse[c], J.-L. Dirion[b], M. Debacq[a,*]

[a] *Conservatoire National des Arts et Métiers, CMGPCE (EA7341), 2 Rue Conté, 75003 Paris, France.*
[b] *Université de Toulouse, Mines Albi, CNRS UMR 5302, Centre RAPSODEE, Campus Jarlard, F-81013 Albi cedex 09, France*
[c] *Université de Lyon, CNRS, INSA-Lyon, CETHIL, UMR5008, Centre de Thermique de Lyon F-69621 Villeurbanne, France*

Abstract

Up-scaling tracer experiments were carried out in a pilot-scale rotary kiln twice as big as the kiln used in the first two Parts of this study. Internal fixtures such as grid, or lifter structure arranged in 3 and 6 rows of single throughout lifters were used. The effects of these removable fixtures and other usual operating conditions, namely, mass flow rate of granular biomass materials, rotational speed and slope of the kiln on the residence time distribution (RTD), the mean and variance of residence time (MRT and VRT), the hold-up (HU), the Peclet number (Pe) and corresponding axial dispersion coefficient (D), were investigated. Scaling-up rules were derived for the MRT, HU volume fraction and D from the results of a comprehensive experimental work. Good agreement was found between the experimental data and the calculated values. The wide size distribution of the beech chips used in the present study allows analysis of particle segregation, which may further increase understanding of the flow characteristics of granular materials, notably within flighted rotary kilns. The results show that while significantly increasing the dispersion, ipso facto, enhancing the mixing, the lifters limit the extent of particle segregation.

Keywords: Rotary kiln, RTD MRT, Filling degree, Axial Dispersion, Lifters, Particle segregation

1. Introduction

Rotary kilns have become over the years among the most commonly used gas-solid reactors in a variety of applications in metallurgical and chemical manufacturing, but also in the waste disposal. They are equally applicable to a wide range of materials ranging from granular solids to sludge and slurry. In the processing of solids, the particle size distribution is only a function of the handling capacity of the feeding system.

The focus of this study, initiated in [1, 2], is the characterization of solids transport within flighted rotary kilns. If there have been several studies in that field up-to-date, most of these studies have generally focused on the bare kiln [3–6] to model through empirical or mechanistic correlations some of the main solids transport variables such as the hold-up, mean residence time or the bed depth profile. A few studies have characterized effect of the lifters on the flow of solids particles [7–11].

The correlations developed by Hwan [12] for horizontal flighted rotary kilns can be mentioned. They are based on dimensional analysis similar to the correlation by Chatterjee et al. [13], which was adjusted using residence time distribution (RTD) measurements conducted in an inclined rotary kiln without lifters but equipped with an exit dam. Hwan [12] performed systematic experiments carried out in horizontal rotary kilns of different length-to-diameter ratios (between 5 and 10), using segmented lifters and different solid materials. From these

*Principal corresponding author
Email address: marie.debacq-lapassat@cnam.fr (M. Debacq)

results, the following equations were established respectively for the prediction of the volumetric filling degree, f, the time of passage, τ, and the axial dispersion coefficient, D:

$$f = 10.91\theta^{1.14}\left(\frac{d_p}{D_i}\right)^{-0.15}\left(\frac{\rho\omega D_i^2}{\dot{M}/D_i}\right)^{-0.90}\left(\frac{\omega^2 D_i}{g}\right)^{-0.03}\left(\frac{h_l}{D_i}\right)^{-0.52}\left(\frac{L}{D_i}\right)^{-0.40} \quad (1)$$

$$\tau = 8.57\frac{\rho L D_i^2}{\dot{M}}\theta^{1.14}\left(\frac{d_p}{D_i}\right)^{-0.15}\left(\frac{\rho\omega D_i^2}{\dot{M}/D_i}\right)^{-0.90}\left(\frac{\omega^2 D_i}{g}\right)^{-0.03}\left(\frac{h_l}{D_i}\right)^{-0.52}\left(\frac{L}{D_i}\right)^{-0.40} \quad (2)$$

$$\mathrm{D}^2 = 0.12\frac{\dot{M}}{\rho u}\theta^{-1.14}\left(\frac{d_p}{D_i}\right)^{0.15}\left(\frac{\rho\omega D_i^2}{\dot{M}/D_i}\right)^{0.90}\left(\frac{\omega^2 D_i}{g}\right)^{0.03}\left(\frac{h_l}{D_i}\right)^{0.52}\left(\frac{L}{D_i}\right)^{0.40} \quad (3)$$

where θ is the angle of repose, d_p is the particle mean diameter, ω is the angular speed, h_l is the lifter height, and u is the axial solids velocity. Unsurprisingly these models suggest that the three solids transport coefficients f, $\frac{\tau\dot{M}}{\rho L D^2}$, and $\frac{\dot{M}}{\rho u \mathrm{D}^2}$ are dependent of same parameters, however, in the present case they may vary exactly in the same way for the identified set of dimensionless groups, only differing by a multiplication factor.

To further understanding of the flow of materials in inclined flighted rotary kiln units started in Parts I and II, in the present work , granular materials (biomass) of wider size distribution, and a rotary kiln of larger scale were used. As will be presented in the following sections, the present study aims at investigating the effects of lifter shape and configurations, kiln rotational speed and slope, and mass flow rate on:

- the RTD of solid particles, determined from experimental stimulus response test; and the corresponding mean and variance of residence time (MRT and VRT);
- the hold-up (HU) of solid particles;
- the Peclet number (Pe) as well as the corresponding axial dispersion coefficient (D);
- the segregation of solid particles.

A set of models are proposed for the prediction of the MRT, HU (volume fraction) and D. These models, established on the basis of dimensional considerations, can be used either for design or control purposes.

2. Materials and methods

2.1. Apparatus and materials

The pilot scale rotary kiln considered to carry out this study consists of a tube made of an nickel-chromium alloy. The tube, supported on rollers, is 4.2 m in length and 0.21 m in diameter. It can be tilted from 0° and downward to an angle of 7°. The kiln tube can be rotated between 0.5 and 21 rpm through chains and sprockets coupled to a variable speed motor. At the upper end of the tube, the feeding system comprising a 30 L hopper and a vibrating cylindrical conveyor is set up. At the lower end, it is possible to install (in a sealed manner, if necessary) a tank (30 L) for storage. Notice that the feed rate is adjusted by regulating the vibration frequency of the conveyor on the basis of continuous weight measurements of the feeding system by an electronic balance. A second electronic balance is installed at the kiln end, so that both inlet and outlet mass flow rates can be continuously determined.

The smooth inner wall of the kiln tube can be equipped with a grid or a lifter structure. These features are illustrated in Figure 1. The grid consists of 16 rows of thin rods (5 mm in diameter) equally distributed in the periphery as shown in Figure 1a. The lifter structure can hold, depending on the desired configuration, a maximum of 36 one-section lifters (30 mm), referred to as straight lifters (SL). The lifters can be longitudinally

arranged in a maximum of six rows equally distributed in the periphery: either as single throughout lifters or segmented lifters. The configurations used in this study are represented in Figure 1b: 3 and 6 rows of single throughout lifters. The main characteristics of the rotary kiln and the order of magnitude of operating conditions investigated in the present work are summarized in Table 1.

Biomass materials are selected to run the experiments; specifically, beech chips are chosen. A characterization of the size distribution of these particles is achieved using 250 particles randomly chosen among tracer particles used for the RTD experiments. The size distribution of these free flowing parallelepiped chips is quite wide as illustrated in Figure 2: 5-17 mm in length, 2-8 mm in width and 1-4 mm in thickness. In addition, as shown in Table 2, the materials used are characterized by a bulk density, ρ_{bulk}, about 260 $\pm$ 30 kg.m^{-3} and a repose angle, θ, about 42 $\pm$ 1° measured through the fixed cone method [14].

A comparison with the rotary kiln used in [1, 2] shows that the two pilot-scale rotary kilns share a very similar length-to-diameter ratio. However, looking at their dimension ratio, there is a factor about two. The particles size used in the present study is an order of magnitude higher and of a wider distribution compared to those of the sand (0.55 mm) and broken rice (3.8 mm $\times$ 1.9 mm) particles used in the first Parts [1, 2].

2.2. Experimental procedure

The experiments conducted in the present study were performed at ambient temperature and atmospheric pressure. The RTD measurement procedure was kept as close as possible to the one presented in Bongo Njeng et al. [1]. However, the feeding systems of these units being different, the impulse injection was carried out differently. In order to characterize the flow of beech chips, stimulus response tests are performed using dyed beech chip tracers as emphasized above, following the procedure outlined below:

Step 1: The desired internal fixture is installed at the inner wall, if necessary. The kiln tube is then tilted to the desired angle value. Then the rotational speed and mass flow rate are indicated on the user interface of the operating unit. The rotary kiln is then started and the feed hopper regularly filled with biomass materials to keep it topped up, when needed.

Step 2: Steady-state conditions of the flow are reached, usually after 2-4 hours. The steady-state conditions are assumed to be reached when: the slopes of the lines obtained by plotting the mass variations with time at inlet and outlet, are equal. In addition, the measured inlet and outlet mass flow rates must be equal within a margin of $\pm$0.05 kg.h^{-1}.

Step 3: The unit is then run until emptying the hopper. The kiln tube inlet end is not readily accessible. Hence, when the vibrating conveyor was empty, the system was stopped to perform the tracer injection. A known amount of dyed beech chips is injected at the kiln inlet end through the hopper and the vibrating conveyor, while the system is stopped. The feed hopper is then refilled with the beech chips and the whole unit is started again at an arbitrary zero time.

Step 4: Samples are then continuously collected at the kiln outlet end with a sampling time of 30 s until all tracer materials are (visually) discharged. The sample time was reduced to 15 s when the tracer particles tended to exit the kiln in a very short time.

Step 5: Then, the kiln rotation is stopped and the vibrating conveyor disabled at the same time. Only the kiln rotation is started again and the solids are discharged. The collected solids which constitute the kiln hold-up are weighed.

Step 6: Lastly, the tracer concentration in each sample is determined by weighing on the one hand the collected sample and on the other hand the dyed tracer, manually extracted from the sample. While analyzing the collected samples, the number of dyed tracer particles extracted from each sample is also determined.

It is important to assess the amount of tracers required to provide sufficient accuracy for the RTD analysis. Therefore, preliminary experiments were performed using amounts of dyed beech chips varying from 5 g to 30 g. It was found that amounts of 20 and 30 g of tracers are enough to get a good accuracy. To shorten the sampling analysis time, 20 g of tracers (about 720 particles) are used to perform the RTD measurements.

2.3. Data processing

Data evaluation

The RTD curve or E-curve, E(t), the mean residence time (MRT), $\bar{t}$, and the variance of residence times (VRT), σ^2, are determined as follows [15]:

$$E(t_i) = \frac{\mathrm{C(t)}}{\int_0^\infty \mathrm{C(t)}dt} \cong \frac{\mathrm{C(t_i)}}{\sum_i^{N_S} \mathrm{C(t_i)}\Delta t_i} \tag{4}$$

$$\bar{t} = \frac{\int_0^\infty t\mathrm{C(t)}dt}{\int_0^\infty \mathrm{C(t)}dt} \cong \frac{\sum_i^{N_S} t_i\mathrm{C(t_i)}\Delta t_i}{\sum_i^{N_S} \mathrm{C(t_i)}\Delta t_i} \tag{5}$$

$$\sigma^2 = \frac{\int_0^\infty (t-\bar{t})^2\mathrm{C(t)}dt}{\int_0^\infty \mathrm{C(t)}dt} \cong \frac{\sum_i^{N_S} {t_i}^2\mathrm{C(t_i)}\Delta t_i}{\sum_i^{N_S} \mathrm{C(t_i)}\Delta t_i} - \bar{t}^2 \tag{6}$$

where t is the time, C(t) represents the tracer concentration at the kiln exit end, the time integral of C(t) represents the total tracer concentration, and Δt_i is the sampling time with i=$\{1, 2, 3,..., N_s\}$, N_s is the total number of collected samples.

The presented E(t) function and VRT can also be expressed in dimensionless form using the dimensionless time, $\theta = \frac{t}{\bar{t}}$, as follows: $\mathrm{E}(\theta) = \bar{t}\mathrm{E}(t)$, and $\sigma_\theta^2 = \frac{\sigma^2}{\bar{t}^2}$.

Axial dispersion model

As shown in [1], the axial dispersion model can be used to represent the time dependent E-curves. This model is used to fit the RTD measurements assuming open-open boundary condition. In dimensionless form, the model is given as follows [15]:

$$E(\theta) = \frac{1}{2}\sqrt{\frac{Pe}{\pi\theta}}\exp\left\{-\frac{Pe(1-\theta)^2}{4\theta}\right\} \tag{7}$$

The variance of this distribution is defined as:

$$\sigma_\theta^2 = \frac{2}{Pe} + \frac{8}{Pe^2} \tag{8}$$

The Peclet number, Pe, is then determined by a fitting method that consists in minimizing the deviation between the experimental E-curve and the prediction. The fitted Peclet numbers obtained, and the theoretical Peclet numbers determined from Eq.8, are compared in Figure 3. Except in isolated cases (2 in total), where the least-square algorithm used failed to find the actual Peclet number that represents the experiment, it was found that the theoretical Peclet Number underestimates the actual Peclet number. A similar observation was previously made in [1] while processing sand and broken rice; however in this case the discrepancy observed is smaller. Nevertheless, for the analysis, only results obtained from the fitting method are considered.

Figure 3 also displays a comparison of the experimental MRT from Eq.5 versus the fitted MRT, which is obtained when fitting the experimental data using the dimensional form of Eq.7, i.e., $E(t) = \frac{1}{2}\sqrt{\frac{Pe}{\pi \bar{t} t}} \exp\left(-\frac{Pe(\bar{t}-t)^2}{4\bar{t}t}\right)$. Very good agreement is found. Lastly, in Figure 3 is presented a comparison of the axial dispersion determined from the theoretical and fitted Peclet number using the following expression: $D = uL/Pe$, where $u = L/\bar{t}$ estimates the solids axial velocity. D is inversely proportional to Pe, so that the observed discrepancies show this time an overestimation of the actual axial dispersion coefficient by the theoretical coefficient.

3. Results and discussion

The experimental matrix was derived from a set of benchmark values of the operating parameters defined as follows: a rotational speed of 3 rpm, a kiln slope of 2° and a mass flow rate (MFR) of 5 kg.h^{-1} ($\pm$0.05 kg.h^{-1}). While using the grid, the straight lifters, or even without any internal fixtures, the operating conditions were set to the given values except the one whose effect is being evaluated on the beech chips flow. Note that no exit dam was fitted at the kiln exit end, unlike the kiln used in Parts I and II of this study. Moreover, compared with preceding Parts, the benchmark value of the mass flow rate is doubled, so that the actual kiln can be operated design-loaded or over-loaded depending on the other operating conditions. In addition, the present paper investigates in particular effect of the configuration of lifters, arranged as 3 or 6 rows of single throughout lifters; effect of the grid on the flow behavior is also considered. Effect of the operating parameters on the flow characteristics of materials are qualitatively and quantitatively studied through: (1) the residence time distribution (RTD), (2) the mean residence time (MRT), (3) the variance of residence time (VRT), (4) the hold-up (HU), (5) the Peclet number (Pe) and axial dispersion coefficient (D), and (6) the segregation of solids. For this purpose, 28 different runs are performed. The detailed results of the experimental campaign are summarized in Table 5 in the Appendix 5.1.

3.1. Influence of operating variables on the experimental RTD, MRT, VRT and HU

3.1.1. Effect of lifters configuration

Effect of the lifter shape has been previously established while comparing the flow characteristics in a smaller kiln operated with 4 straight and 4 rectangular lifters equally spaced around the kiln tube internal wall periphery. The lifters with higher hold up capacity were found to generate more dispersion and longer residence times. Here the lifters used are similar but two configurations are tested: 3 and 6 rows of single throughout straight lifters. In addition, the effects of a grid are also considered. Figure 4 presents the variations of the residence time distribution when operating at the given benchmark values with and without internal fixtures; the replicated runs are plotted. The RTD curves overlap; in particular, those corresponding to 3SL and 6SL are nearly superimposing. Notice that in the absence of internal fixtures the flow behaves as a plug flow as suggested by the narrow RTD obtained.

Figure 6 presents the variations of mean residence time, filling degree and variance of residence time with the kiln operating conditions for different internal fixtures or without. From the latter, it is clear, except when varying the mass flow rate, that the following order can apply to the experiments considering uncertainties as presented later on:

$$\bar{t}_{NL} < \bar{t}_G < \bar{t}_{3SL} \lesssim \bar{t}_{6SL} \text{ , } \sigma^2_{NL} < \sigma^2_G < \sigma^2_{3SL} \lesssim \sigma^2_{6SL} \text{ and } HU_{NL} < HU_G < HU_{3SL} \lesssim HU_{6SL}.$$

It must be specified that very little or no significant differences were observed in the results obtained with the 3SL and 6SL. However, using lifters significantly increased the kiln hold-up and thus the filling degree, but

also the MRT and VRT, as shown in Figure 6. Still, unlike what might be expected, the results are more or less equal with small discrepancies, especially when the kiln was over-loaded in both 3SL and 6SL configurations. The kiln was over-loaded usually for filling degree higher than 8-10%. In fact, it appears that in the latter condition the amount of solids lifted out of the bulk bed by the lifters is virtually the same while using 3SL or 6SL, and probably would have not been increased much even with 12SL as illustrated in Figure 5. Hence, it is not so much the number of rows of lifters that will affect the flow characteristic but rather the overall hold up capacity of these lifters. Using lifters of (1) higher holding capacity and (2) higher angular position at the end of discharge, such as rectangular lifters, theoretically must have shown greater differences between the lifters configurations mainly because of the overall hold up capacity.

Aside from the evident benefit of increasing the friction at the kiln smooth wall, using a grid helps to promote rolling motion into the bulk bed. This latter motion, well characterized by Henein et al. [16], is most commonly found in kiln operation. It is observed that in runs where no internal fixtures are installed at the kiln internal wall, the bulk bed is in the slipping mode as described by [16, 17], especially when the filling degree is lower than 8%. Experiments show that using a grid at similar operating conditions will set a rolling motion within the bulk bed. In fact, the grid can be considered as a structure of small flights, which continuously scrape off the solids from the bottom of the bulk bed to the upper part of the bed surface. Therefore, the grid imposes a motion en masse at the bottom part of the bed at the kiln rotational speed and generates at the bed surface a steady discharge of solids. This has a significant impact on the HU, MRT and VRT, which are all increased compared to the case of a smooth internal wall. However, this is still a moderate increase compared to the large increase induced by the use of lifters because of differences in size and holding capacity.

3.1.2. Effect of operating parameters: rotational speed, kiln slope and mass flow rate

Figure 7 shows the influence of the operating parameters on the residence time distribution of beech chips when the kiln is equipped with 6 rows of single throughout lifters. A general remark that can be made on the obtained RTD curves over the whole experimental campaign is the presence of small peaks extending the tail of the distributions. This can be due to some particle segregation phenomena occurring in the bulk bed as discussed later. The results presented in the following sections are also analyzed in the scope of previous observations made on the flow characteristics of sand and broken rice.

Kiln rotational speed. Similar to previous observations, there is a sharp decrease of the MRT by about 70% as the rotational speed is increased from 2 to 6 rpm (see Figure 6a). That increase is also suggested by the shifting of the RTD curves toward lower residence times (see Figure 7). However, unlike previous observations, the shape of the curves significantly changes from a spread distribution with a low peak to a very narrow distribution with a high peak. This is confirmed by the sharp decrease in the VRT (see Figure 6c). Finally, the kiln hold up is also decreased, actually divided by 3 to 4, when the kiln rotational speed varies from 2 to 6 rpm (see Figure 6b). Indeed with higher rotational speed the solids flow in the kilning bed or through lifters is faster, so that the accumulation of solids in the burden is reduced.

Kiln slope. The kiln slope has a similar effect to that of the kiln rotational speed on the flow of beech chips. The same trends were previously observed while operating sand or broken rice. When increasing the kiln slope, whether the motion within the bulk bed is slipping or rolling, the forward axial displacement of solids is significantly increased due to gravity. In the first case, it is observed that the bed adheres to the rotating wall, up to a certain angle of deflection as described by Mellmann [17], and then en masse, the bed slides back and

forward along the kiln slope. In the second case, when rolling motion is achieved, the particles thrown off the apex of the bed flow down along the bed inclination but also forward following the kiln slope. The higher the kiln slope, the higher the particles forward displacement. As a result an increase in the kiln slope reduce the MRT and filling degree, as illustrated respectively in Figures 6a and 6b. As shown in Figure 7, the RTD shapes also vary much from widespread distribution to narrow distribution with increasing kiln slope, as indicated by the decrease of the VRT in Figure 6c.

Mass flow rate. Surprisingly, the mass flow rate has little effect on the flow of beech chips, as implied by the quasi overlapping RTD curves (see Figure 7). Even if a similar trend was observed previously while using broken rice, the rate of increase of the MRT with flow rate was higher than that of the present materials (see Figure 6a). In addition, significant changes in the shape of RTD curves were reported for the flow of sand and broken rice. The observed divergence can be related to the materials properties, rather than a difference in the tracer pulse experiment procedure, or even the amount of tracer with regard to the bulk burden. Notice that the VRT is strongly influenced by the type of motion of the bulk bed (see Figure 6c). Large discrepancies can be observed with regard to runs in slipping mode (without lifters or grid). When operating in rolling motion, if the MRT and VRT remain almost constant, the filling degree significantly increases linearly with the mass flow rate (see Figure 6b). This latter results are important for kiln operation, since they imply that the bulk burden can be significantly increased, without, this requiring much more residence time within the kiln.

3.2. Influence of operating variables on the experimental Pe and D

Figure 8 represents the variations of the Peclet number and resulting axial dispersion coefficient with the kiln operating conditions, when equipped with internal fixtures. The runs without internal fixtures, which display slipping motion, are not represented in order to focus only on the results referring to the rolling motion.

The Peclet numbers, determined by fitting the RTD curves, are large and comprise between 200 and 800 for runs in rolling motion, and even higher in case of slipping motion (see NL in Table 5). Indeed the higher the Peclet number, the smaller the dispersion, which thereby promotes plug flow. The Peclet number and axial dispersion have been previously investigated by several authors [5, 18–20], concluding most of the time that the Peclet number increased with rotational speed and slope of the kiln, and remained constant with the flow rate. However the present results do not all agree with these previous findings. Among the internal fixtures, the grid, which induces lower filling degree, shows higher Peclet number, and thus generates lower longitudinal back-mixing compared to the 3SL and 6SL configurations. It can be seen that when using the grid, the Peclet number decreases with the rotational speed, but that it remains fairly constant within the experimental error for the 3SL and 6SL configurations. A previous analysis of the flow of sand and broken rice shows, in accordance with the actual results, that the Peclet number increases with the mass flow rate; but unlike previous results, it is observed in this case while investigating the flow of beech chips that the Peclet number increases with the kiln slope.

The values reported in the present study for the axial dispersion coefficient are in the order of magnitude of those reported for the sand and broken rice in Part I, but also with those reported by Wes et al. [21] ($4 \cdot 10^{-5} \mathrm{m}^2.\mathrm{s}^{-1}$) or Sai et al. [5] ($2 \cdot 10^{-5} \mathrm{m}^2.\mathrm{s}^{-1}$). Furthermore the observed trends are similar to those previously described: the axial dispersion coefficient is found to increase with rotational speed and slope of the kiln, but to decrease with the mass flow rate. It can be added that higher dispersion coefficient values are obtained for the 3SL and 6SL configurations, as expected. Note that the axial dispersion coefficient increases

as the filling degree decreases for a given internal fixture. Indeed, the mixing effect is much more powerful in a lower bulk burden than in a large one.

3.3. Modeling: MRT, HU and D

In this section are presented some scale-up rules for flighted rotary kilns. Models are determined from dimensional considerations for the prediction of the mean residence time, the filling degree and the axial dispersion. The dimensionless groups presented in the following sections may not account for inter-particle forces that may occur between cohesive particles. They may primarily be appropriated for free-flowing particles whose size may vary between 0.4 and 15 mm. In addition, they may likely be applicable to the rolling mode. The following scale-up rules are derived from previous findings in the literature as well as from experimental results obtained in this study while processing sand, broken rice and beech chips. The main operating parameters, geometrical characteristics and physical properties, that may affect the MRT, the HU volume fraction and D are listed as follows: the rotational speed (N), the mass flow rate ($\dot{\mathrm{M}}$), the kiln slope (S), the exit diameter (D_{ex}), the cross section of materials in lifters ($\mathrm{S}_{\mathrm{lift}}$), the length of the kiln (L), the internal diameter of the kiln (D_i), the bulk density of materials (ρ_{bulk}), the tapped density of materials (ρ_{tapped}), the angle of repose of the bulk materials (θ), the particle equivalent size ($\mathrm{d_p}$), and the gravitational acceleration (g). Note that: (1) $S_{lift} = \frac{\pi D_i^2}{4} - \frac{n_{lift}-1}{2} S_{horlift}$ with n_{lift} the total number of lifters and $S_{horlift}$ the section of materials in a lifter at horizontal position, which can be determined using the materials angle of repose and lifters dimensions [22–24], (2) $d_p = \sqrt[3]{l_l l_w l_t}$ with l_l, l_w and l_t respectively the particles average length, width and thickness.

From the defined variables, following a procedure that can be found in [25], dimensionless groups are set to correlate the MRT, HU[%] and D as follows. Table 3 summarizes the values of the model parameters determined with the use of experimental data at the 95% confidence level, while Figure 9 presents the comparison of the calculated model predictions with experimental results.

3.3.1. MRT

The model established for the mean residence time is presented in Eq.9. This might be very similar to the previous proposition in Part II, but there are a few differences. In order to define the dimensionless groups, it is necessary to choose a set of parameters to represent the fundamental dimensions. In this study the involved dimensions are mass, length and time. To achieve the dimensional analysis in this paper ρ_{bulk}, D_i and g are selected, instead of ρ_{bulk}, D_i and N in Part II of this study. This allows the impact of the operating parameter N to be set in only one dimensionless group: the Froude number. The dimensionless parameters, θ and S, are gathered in one group. Finally, the model parameters presented in Table 3 are determined from experimental results obtained from the 3 granular materials used: sand, broken rice and beech chips. Notice that these parameters are determined within narrow confidence intervals.

$$\bar{t} = k\sqrt{gL}\left(\frac{N^2 D_i}{g}\right)^{\alpha}\left(\frac{D_{ex}}{D_i}\right)^{\beta}\left(\frac{\theta}{S}\right)^{\gamma}\left(\frac{\dot{M}}{\rho_{bulk} D_i^2\sqrt{gL}}\right)^{\delta}\left(\frac{4S_{lift}}{\pi D_i^2}\right)^{\epsilon}\left(\frac{\rho_{bulk}}{\rho_{tapped}}\right)^{\zeta}\left(\frac{L}{D_i}\right)^{\eta} \quad (9)$$

Unlike previous results in Part II [2] or by Hwan [12] in the literature, it is found that the Froude number has a significant impact on the MRT. As illustrated in Figure 9a, the predictions from Eq.9 are in good agreement with the experimental data irrespective of the kiln or the materials used. For the calculations, the variables forming the dimensionless groups must be filled in SI units, therefore the unit of the obtained predictions for

the MRT is second. Notice that in the present study the length-to-diameter ratio varies only slightly and could not be used for parameter fitting, therefore the value of η is set to 1.1, which has been previously determined by Chatterjee et al. [13].

3.3.2. HU

The model defined for the filling degree is presented in Eq.10. It is very similar to the one proposed for the MRT. Indeed a direct correlation can be found between these two, especially when the dispersion is very negligible, the time of passage and the mean residence time are very close, yet the time of passage is defined as $\tau = HU/\dot{M}$. This also explains why some parameters of both models are very close, such as α, β, and γ, as shown in Table 3.

$$HU[\%] = k\frac{\rho_{bulk} L \pi D_i^2}{4}\left(\frac{N^2 D_i}{g}\right)^{\alpha}\left(\frac{D_{ex}}{D_i}\right)^{\beta}\left(\frac{\theta}{S}\right)^{\gamma}\left(\frac{\dot{M}}{\rho_{bulk} D_i^2\sqrt{gL}}\right)^{\delta}\left(\frac{4S_{lift}}{\pi D_i^2}\right)^{\epsilon}\left(\frac{\rho_{bulk}}{\rho_{tapped}}\right)^{\zeta}\left(\frac{L}{D_i}\right)^{\eta} \tag{10}$$

Note that the model parameters were not only determined using the hold-up measurements from this hydrodynamic study; the hold-up measurements obtained while performing experiments at hot temperatures with sand were also used [26], as illustrated in Figure 9b. The model parameters were defined within narrower confidence intervals, and good agreements were found between the calculated and experimental filling degree. To obtain the filling degree, the variable parameters must be filled using SI units; the model directly produces a percentage. Note that the value of the parameter η is fixed to 0, since no fitting value was found in the literature that was defined with sufficient accuracy for the length-to-diameter ratio.

3.3.3. D

The proposed model for the axial dispersion coefficient is given in Eq.11. The materials physical properties have been reported to significantly affect the axial dispersion coefficient. They are represented in the given model by the Hausner ratio, as well as a ratio of the particle equivalent size to the kiln diameter. The model parameters are determined within reasonable confidence intervals as given in Table 3.

$$D = k\sqrt{D_i^2 gL}\left(\frac{N^2 D_i}{g}\right)^{\alpha}\left(\frac{d_p}{D_i}\right)^{\beta}(S)^{\gamma}\left(\frac{\dot{M}}{\rho_{bulk} D_i^2\sqrt{gL}}\right)^{\delta}\left(\frac{4S_{lift}}{\pi D_i^2}\right)^{\epsilon}\left(\frac{\rho_{bulk}}{\rho_{tapped}}\right)^{\zeta}\left(\frac{L}{D_i}\right)^{\eta} \tag{11}$$

Figure 9c shows that all experimental data do not agree well with the predicted value within the $\pm 20\%$ margins. However, as shown later on, these predictions are mostly within the experimental uncertainty which is about 30%. Except scarce cases in particular for beech chips, the experimental data obtained without internal fixture are not well predicted by the model, certainly because of a bed flowing in the slipping mode. Note that η is fixed to 0. Therefore the effect of the length-to-diameter ratio is taken into account within the value of the model parameter k.

3.4. Analysis of particle segregation

Segregation is a property of dry granular solids, which tend to separate spatially by size, shape or density under varying flow conditions [27, 28]. This phenomenon has been observed in industrial processing involving granular materials, and it has been widely studied within rotating drums.

In this study, there are a few elements that may indicate possible phenomena of segregation. Firstly, the wide size distribution of beech chips, as illustrated in Figure 2, indeed implies not only larger or smaller particles but also heavier and lighter particles. Generally, the larger the chip size, the heavier the chip weight. Secondly, while analyzing the beech chips RTD curves, an extended tail can be observed due to small peaks of tracer concentration, implying a possible higher concentration due to particle segregation.

Bensmann et al. [29] has been able to investigate the particle segregation through tracer experiments using several fractions of tracers particles. With such a straightforward approach, the effects of segregation can be easily observed and analyzed. However as previously demonstrated by Colin et al. [30] such experiments are not mandatory. Instead, a tracer of wide distribution size (see Figure 2) can be used to achieve this purpose. As stated before, while analyzing the samples collected after the tracer injection, the number of tracer particles contained in each sample was determined. From the number of tracer particles collected and their weight, an average particle weight can be determined and is used for the analysis of particle segregation. The present analysis is therefore less in terms of particle size and more in terms of particle weight, due to the direct relationship. Note that there have been good tracer mass recoveries as follows, for NL experiments 99.5% $\pm$ 0.5, for G experiments 99.4% $\pm$ 0.7, for 3SL experiments 99.3% $\pm$ 0.6 and for 6SL experiment 99.9$\pm$0.6%.

Figure 10 presents the (dimensionless) time variations of the average tracer weight for a variety of operating conditions when using a grid, 3SL, 6SL and no internal fixtures. A first preliminary general observation concerns the unbalanced distribution of tracer around the mean residence time symbolized by the red line, which furthers understanding of the presence of an extended tail on the RTD curves. It is also observed that the average weight of tracer particles is mainly between 20 and 30 mg. Out of this interval the particles can be considered lighter or heavier and by extension smaller or larger. Assuming a beech chip of parallelepiped shape, about 10 mm $\times$ 4.5 mm $\times$ 2 mm, and a density of 279 kg.m^{-3}, the particle weight is about 25.1 mg.

A more detailed look in Figure 10 demonstrates that when varying only one operating condition and keeping the other constant, the obtained weight distribution differed primarily in function of the filling degree as highlighted by Colin et al. [30]. Secondly it is also observed that the tracer average weight distribution varies depending on presence and type of internal fixtures.

In Figures 10a, b and c, where there is no internal fixtures, there is no significant effect of segregation at low filling degree (below 8%): distributions are more centered, with a tracer weight remaining nearly constant in spite of few lighter and heavier particles respectively at lower and larger residence times. Whereas at higher filling degree, the tracer average weight distribution is more dispersed and the heavier particles tend to have significantly lower residence time compared to lighter particles. This can be explained by the differing mode of motion observed at lower and higher filling degree, respectively, slipping motion and rolling motion. From the literature [27], it is well known that especially in the rolling motion, radial segregation may appear very quickly, causing concentration of smaller particles toward the core of the bed, while larger particles may roll in the active layer following the incline at the bed surface. Knowing that the axial transport is highly promoted by the continuous flow at the bed surface, this may explain the preceding observations.

When a grid is used as shown in Figures 10d, e and f, the tracer average weight decreases slowly with time, implying higher concentration of heavier particles at low residence time and higher concentration of lighter particles at high residence time as previously observed in case of rolling motion. It seems that the grid tends in a way to homogenize the bulk of particles. That homogenization can also be observed when using 3SL or 6SL. In both latter cases, except at higher residence times, the weight distribution is not widespread, and there is

no more a decrease in the tracer average weight. These observations may be related with Grajales et al. [31] statements implying that straight lifters do not affect the flow regimes of the kilning bed but only reduce the area of the central core in the rolling motion. Hence, the concentration of small particles in the core at the bed center is reduced, and the small particles are allowed to flow with the bigger particles in the active layer. This reduces the time of residence of smaller particles, therefore lowering the tracer average weight at lower residence times, and by scarcity effect (of lighter particles) automatically increases the tracer average weight at higher residence times, as shown in Figures 10g, h and i when using 3SL, and in Figures 10j, k and l when using 6SL.

However, the presence of heavier particles at higher residence time can be possibly due to effect of axial segregation [28], which unlike radial segregation is reported to develop after hundreds of kiln rotations. Therefore the axial segregation, happening after radial segregation, splits the existing core into periodic axial band along the kiln axis. This may also explained in some cases the extensive presence of heavier particles at higher residence time.

3.5. Reproducibility of experiments

Reproducibility of the experimental results was investigated through replicates of some runs. Table 4 shows the experimental hold-up, mean residence time, variance of residence time, Peclet number and axial dispersion coefficient determined. Figure 11 illustrates the reproducibility of the segregation of particles. Both Table 4 and Figure 11 gather the results of the replicates of some runs carried out at selected benchmark values for the operating conditions, when the kiln was equipped with 3 and 6 rows of straight lifters, and without internal fixture.

In Table 4, the given values of the relative uncertainty for the hold up and MRT are lower than 6%, implying very good reproducibility of these two flow characteristics. The reported relative uncertainties for the VRT, Pe and D are higher, reaching 30% at maximum. For decision making in industry, even if these uncertainties are relatively high, they are sufficiently low to consider the experimental values as consistent. Note that the relative uncertainties derived from the replicates are determined at the 80% confidence level.

In Figure 11, the reproducibility of the experiments is very good in terms of uniform repartition of more and less dense tracer particles along the dimensionless time. This confirms also the reproducibility of RTD experiments as illustrated in Figure 4.

4. Conclusions

The flow characteristics of materials are significantly impacted by the internal fixtures. Therefore, in the design stage or for improvement purposes, the choice of lifters' configuration as well as their overall holding capacity, mostly dependent on the shape, must be carefully selected. The use of lifters increases the burden and the residence time of solid particles. They promote the mixing of particles as suggested by the increase of the axial dispersion coefficient. In regard to the flow of materials of wide size distribution, by their mixing effect, lifters reduce the segregation phenomena that may occur, causing different residence time for the different size fractions.

The flow characteristics of solids through flighted rotary kilns are also affected by the operating conditions as demonstrated by the experimental results:

- Increase in the mean residence time may result from a decrease of the rotational speed and slope of the kiln, but also to a lesser extent, from an increase in the mass flow rate of solids;

- The mass flow rate has a remarkable influence on the filling degree. As the flow rate is increased, or the kiln rotational speed and slope are decreased, the hold-up increased.

- The axial dispersion is increased with the kiln rotational speed and slope, but decreased with the mass flow rate. The higher the filling degree the smaller the axial dispersion.

Three models were developed for the prediction of the mean residence time, the filling degree, and the axial dispersion coefficient under steady-state conditions in inclined rotating kilns, whether equipped with lifters and exit dams or not, and operated in the rolling mode. These correlations consist of dimensionless factors accounting for (1) the basic operational parameters of the kiln, (2) the properties of the bulk solids, (3) the geometry of the kiln, (4) the overall lifters' holding capacity, (5) the height of exit dam. The model parameters, namely k, $\alpha, \beta, \ldots, \zeta$ as given in Table 3, have been determined from experimental data of the flow of sand, broken rice and beech chips, at varying operational conditions and through different rotary kilns. The predictions and experimental data were in good agreement.

The segregation analysis made on the flow of beech chips revealed a possible effect of radial segregation. However, it was found that the segregation was lessened in some operating conditions, in particular when using lifters, depending on the filling degree of solids within the kiln.

List of symbols

av.	Average	-
C	Tracer concentration	g/g,
D	Axial dispersion coefficient	$m^2.s^{-1}$
D_{ex}	Effective exit diameter	m
d_p	Particle equivalent size, particle mean diameter	mm
D_i	Kiln internal diameter	m
f	volumetric filling degree	-
g	Gravitational acceleration	$m.s^{-2}$
HU	Hold-up	kg
HU[%]	hold-up volume fraction or filling degree	-
k	Model parameter	-
L	Kiln Length	m
l	Particle size	m
Ls	Area occupied by solid particles contained in loading lifters	m^2
$\dot{M}$, MFR	Mass flow rate	$kg.h^{-1}$
MRT	Mean residence time	min
N	Kiln rotational speed	rpm
NL	No lifters	-
n_{lift}	Total number of lifters	-
N_S	Total number of samples	-
N_T	Total number of experiments	-
Pe	Peclet number	-
RL	Rectangular lifters	-
rpm	Rotation per minute	-
RTD	Residence Time Distribution	-
S	Kiln slope	degrees
SL	Straight lifters	-
S_{lift}	Area covered by solid particles in a lifter at horizontal position	m^2

$S_{horlift}$	Area covered by solid particles in a lifter at horizontal position	m^2
t	Time	min
$\bar{t}$	MRT	min
VRT	Variance of the RTD	min^2

Greek letters

α,β,γ, δ,ϵ,ζ,η	Fitting parameters	-
Δt_i	Sampling times	s
θ	Angle of repose, dimensionless time	degrees, -
ρ_{tapped}	Tapped density	$kg.m^{-3}$
ρ_{bulk}	Bulk density	$kg.m^{-3}$
ρ_{true}	Particle density	$kg.m^{-3}$
σ^2	Variance of residence time	min^2
σ_θ^2	Dimensionless variance of residence time	-
τ	Time of passage	min
ω	Kiln rotational speed	rad/s

Subscripts

G	Grid	-
l	Length	-
NL	No lifters	-
3SL	3 rows of straight lifters	-
6SL	6 rows of straight lifters	-
t	Thickness	-
w	Width	-

5. Appendices

5.1. Experimental Results: HU, MRT, VRT, Pe, D

The experimental matrix achieved and the experimental hold up, mean residence time, and variance of residence time, the fitted Peclet number, and resulting axial dispersion coefficient are resumed in Table 5.

Reference

[1] A. S. Bongo Njeng, S. Vitu, M. Clausse, J. L. Dirion, M. Debacq, Effect of lifter shape and operating parameters on the flow of materials in a pilot rotary kiln: Part I. Experimental RTD and axial dispersion study, Powder Technology 269 (2015) 554–565.

[2] A. S. Bongo Njeng, S. Vitu, M. Clausse, J. L. Dirion, M. Debacq, Effect of lifter shape and operating parameters on the flow of materials in a pilot rotary kiln: Part II. Experimental hold-up and mean residence time modeling, Powder Technology 269 (2015) 566–576.

[3] A. Chatterjee, A. V. Sathe, M. P. Srivastava, P. K. Mukhopadhyay, Flow of materials in rotary kilns used for sponge iron manufacture: Part I. Effect of some operational variables, Metallurgical Transactions B 14 (3) (1983) 375–381.

[4] A. Bandopadhyay, M. P. Srivastava, A. K. Ray, K. K. Prasad, Mathematical modelling of charge movement in rotary kiln for spong iron making, Transactions of the Indian Institute of Metals 39 (3) (1986) 181–186.

[5] P. S. T. Sai, G. D. Surender, A. D. Damodaran, V. Suresh, Z. G. Philip, K. Sankaran, Residence time distribution and material flow studies in a rotary kiln, Metallurgical Transactions B 21 (6) (1990) 1005–1011.

[6] W. Z. Chen, C. H. Wang, T. Liu, C. Y. Zuo, Y. H. Tian, T. T. Gao, Residence time and mass flow rate of particles in carbon rotary kilns, Chemical Engineering and Processing: Process Intensification 48 (4) (2009) 955–960.

[7] C. O. Miller, B. A. Smith, W. H. Schuette, Factors Influencing the Performance of Rotary Dryers, American Institute of Chemical Engineers (1942) 841–864.

[8] J. Kelly, J. O'Donnell, Dynamics of granular material rotary dryers and coolers, in: IChemE Symposium Series, vol. 29, 34–44, 1968.

[9] J. Kelly, Flight design in rotary dryers, Drying Technology 10 (4) (1992) 979–993.

[10] K. Hatzilyberis, G. Androutsopoulos, An Rtd Study for the Flow of Lignite Particles Through a Pilot Rotary Dryer Part II: Flighted Drum Case, Drying Technology 17 (4-5) (1999) 759–774.

[11] D. Ablitzer, H. Henein, A Phenomenological Analysis of Particulate Solids in the Operation of Rotary Reactors, in: Proceedings of the Brimacombe Memorial Symposium, 2000.

[12] I. H. Hwan, Heat transfer mechanisms in an indirectly heated rotary kiln with lifters and its role in scaling, Ph.D. thesis, 2009.

[13] A. Chatterjee, A. V. Sathe, P. K. Mukhopadhyay, Flow of materials in rotary kilns used for sponge iron manufacture: Part II. Effect of kiln geometry, Metallurgical Transactions B 14 (3) (1983) 383–392.

[14] C. R. Woodcock, J. S. Mason, Thames Polytechnic. Bulk Solids Handling Unit, Bulk solids handling: an introduction to the practice and technology, L. Hill ; Chapman and Hall, Glasgow; New York, 1987.

[15] O. Levenspiel, Chemical reaction engineering, Wiley, 1999.

[16] H. Henein, J. K. Brimacombe, A. P. Watkinson, Experimental study of transverse bed motion in rotary kilns, Metallurgical Transactions B 14 (2) (1983) 191–205.

[17] J. Mellmann, The transverse motion of solids in rotating cylinders-forms of motion and transition behavior, Powder Technology 118 (3) (2001) 251–270.

[18] R. Rutgers, Longitudinal mixing of granular material flowing through a rotating cylinder: Part II. Experimental, Chemical Engineering Science 20 (12) (1965) 1089–1100.

[19] A.-Z. Abouzeid, T. Mika, K. Sastry, D. Fuerstenau, The influence of operating variables on the residence time distribution for material transport in a continuous rotary drum, Powder Technology 10 (6) (1974) 273–288.

[20] O. S. Sudah, A. Chester, J. Kowalski, J. Beeckman, F. Muzzio, Quantitative characterization of mixing processes in rotary calciners, Powder Technology 126 (2) (2002) 166–173.

[21] G. W. J. Wes, A. A. H. Drinkenburg, S. Stemerding, Solids mixing and residence time distribution in a horizontal rotary drum reactor, Powder technology 13 (1976) 177–184.

[22] D. Van Puyvelde, B. Young, M. Wilson, S. Schmidt, Modelling Transverse Segregation of Particulate Solids in a Rolling Drum, Chemical Engineering Research and Design 78 (4) (2000) 643–650.

[23] K. R. Sunkara, F. Herz, E. Specht, J. Mellmann, R. Erpelding, Modeling the discharge characteristics of rectangular flights in a flighted rotary drum, Powder Technology 234 (2013) 107–116.

[24] M. Debacq, S. Vitu, D. Ablitzer, J.-L. Houzelot, F. Patisson, Transverse motion of cohesive powders in flighted rotary kilns: Experimental study of unloading at ambient and high temperatures, Powder Technology 245 (2013) 56–63.

[25] G. Delaplace, K. LoubiÃšre, F. Ducept, R. Jeantet, ModÃ©lisation en gÃ©nie des procÃ©dÃ©s par analyse dimensionnelle : MÃ©thode et exemples rÃ©solus, Tec & Doc Lavoisier, Paris, 2014.

[26] A. S. Bongo Njeng, S. Vitu, M. Clausse, J. L. Dirion, M. Debacq, Evaluation of the wall-to-solids and wall-to-gas heat transfer coefficients in flighted rotary kilns: Lumped system analysis, International Journal of Heat and Mass Transfer To be submitted.

[27] F. Cantelaube, D. Bideau, S. Roux, Kinetics of segregation of granular media in a two-dimensional rotating drum, Powder Technology 93 (1) (1997) 1–11.

[28] Z. S. Khan, S. W. Morris, Subdiffusive axial transport of granular materials in a long drum mixer, 2004.

[29] S. Bensmann, A. Subagyo, P. Walzel, Residence Time Distribution of Segregating Sand Particles in a Rotary Drum, Particulate Science and Technology 28 (4) (2010) 319–331.

[30] B. Colin, J. L. Dirion, P. Arlabosse, S. Salvador, Wood chips flow in a rotary kiln: experiments and modeling, Chemical Engineering Research and Design .

[31] L. M. Grajales, N. M. Xavier, J. P. Henrique, J. C. Thomeo, Mixing and motion of rice particles in a rotating drum, Powder Technology 222 (2012) 167, the mixing and motion of particles were analyzed in a rotary drum as part of the developme.

6. Figures

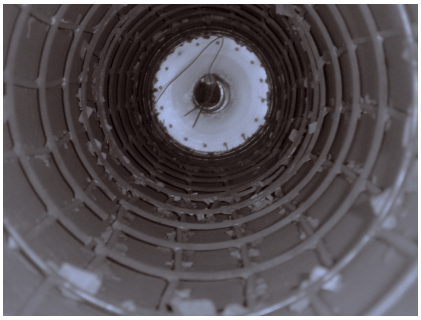

(a) Grid, 16 rows.

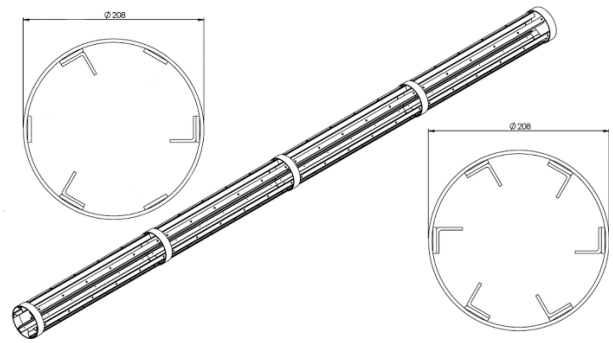

(b) Lifter structure and configurations: 3 rows of SL (left side) and 6 rows of SL (right side).

Fig. 1: Kiln internal fixtures: a) lifter structure and b) grid.

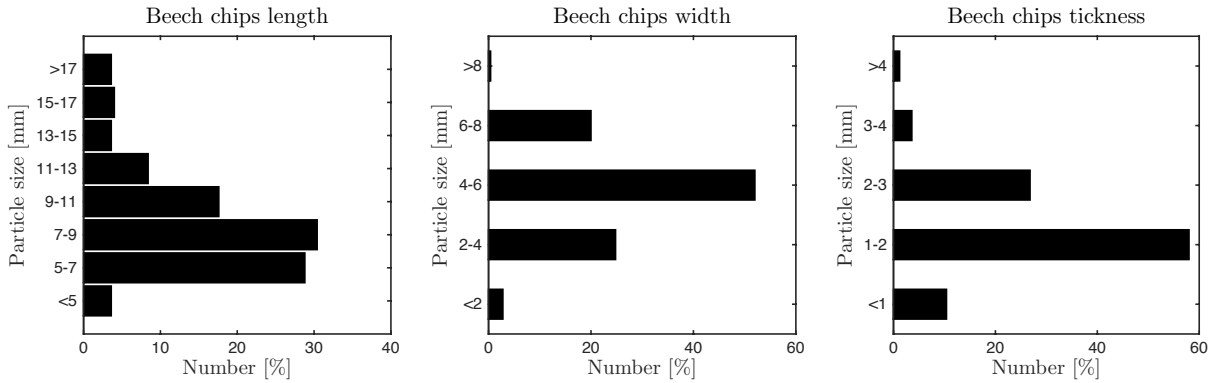

Fig. 2: Beech chips size distribution in length, width and thickness.

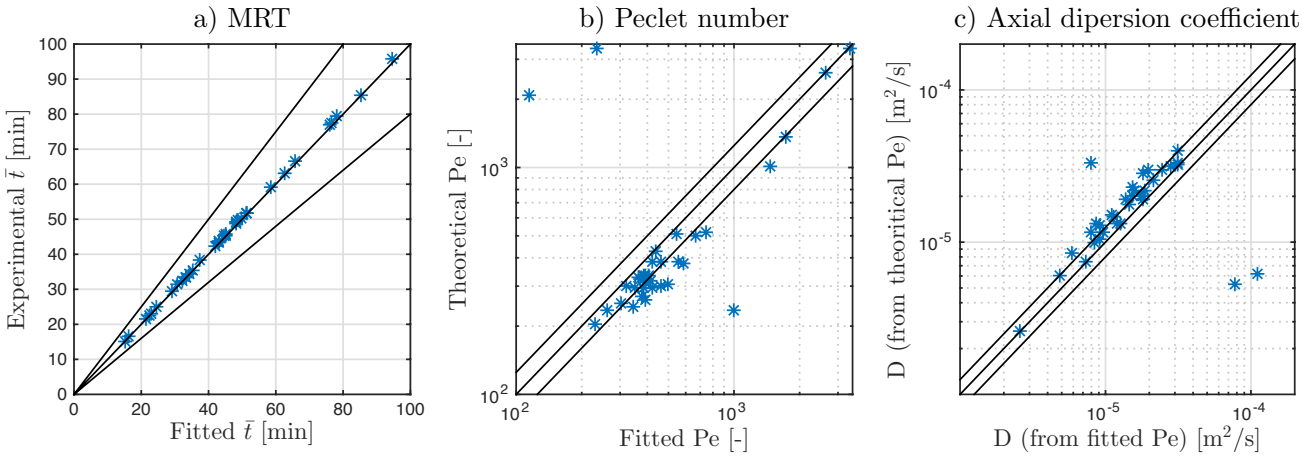

Fig. 3: Comparison of experimental/theoretical and fitted values of the axial dispersion model parameters, i.e MRT, Pe, and resulting D. Solids lines are ±20% margins.

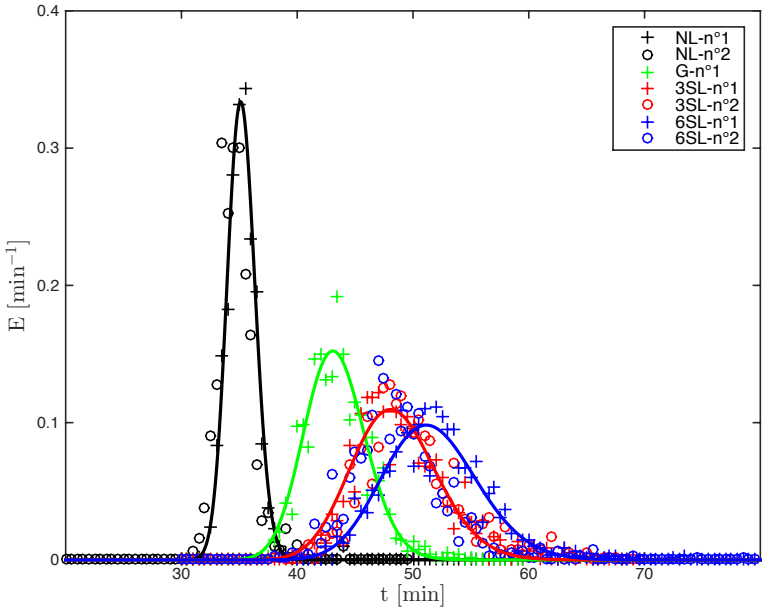

Fig. 4: Effect of lifters configurations on the RTD: no lifters (NL), grid (G), 3 and 6 rows of straight lifters (3SL, 6SL). Operating conditions: 3 rpm rotation speed, 2° slope, 5 kg.h^{-1} MFR. For the runs using NL, 3SL and 6SL, there are 2 replicates. Solid lines are the axial dispersion model of the n°1 replicate.

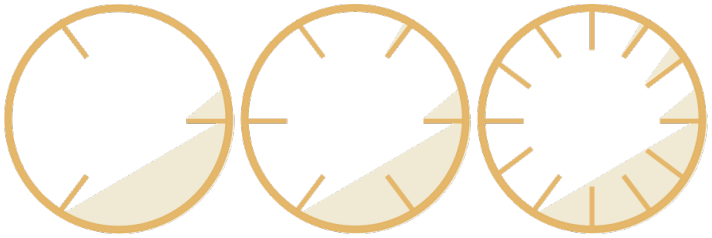

Fig. 5: Lifters hold-up for three configurations, from left to right side: 3SL, 6SL and 12SL.

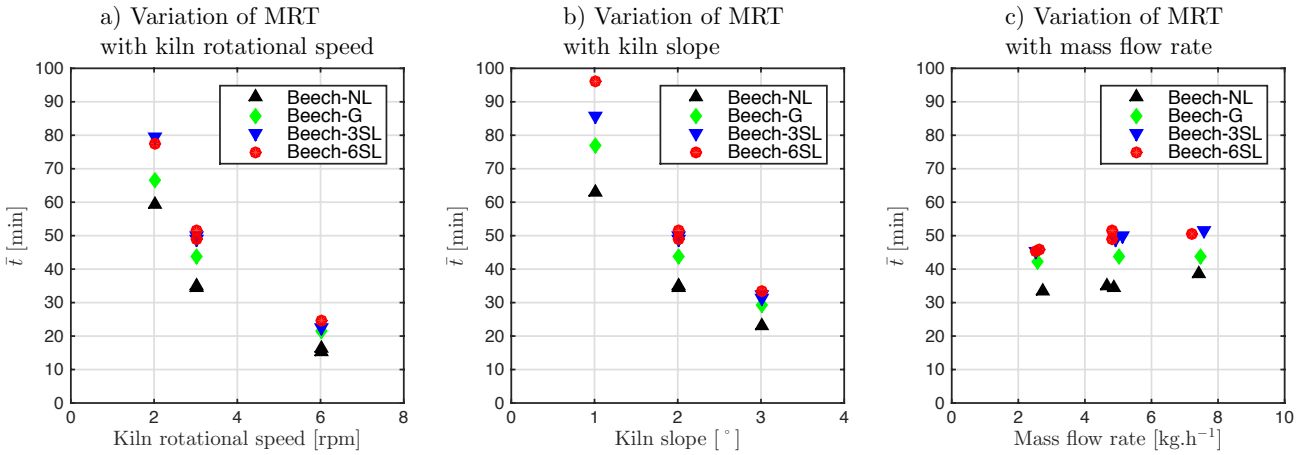

(a) Mean residence time.

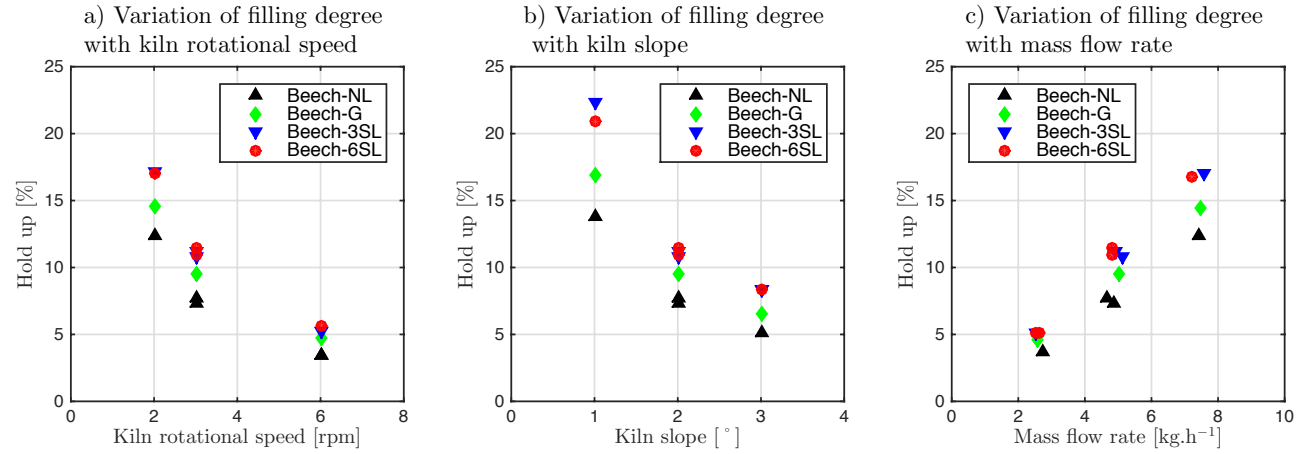

(b) Fractional volumetric hold up (filling degree).

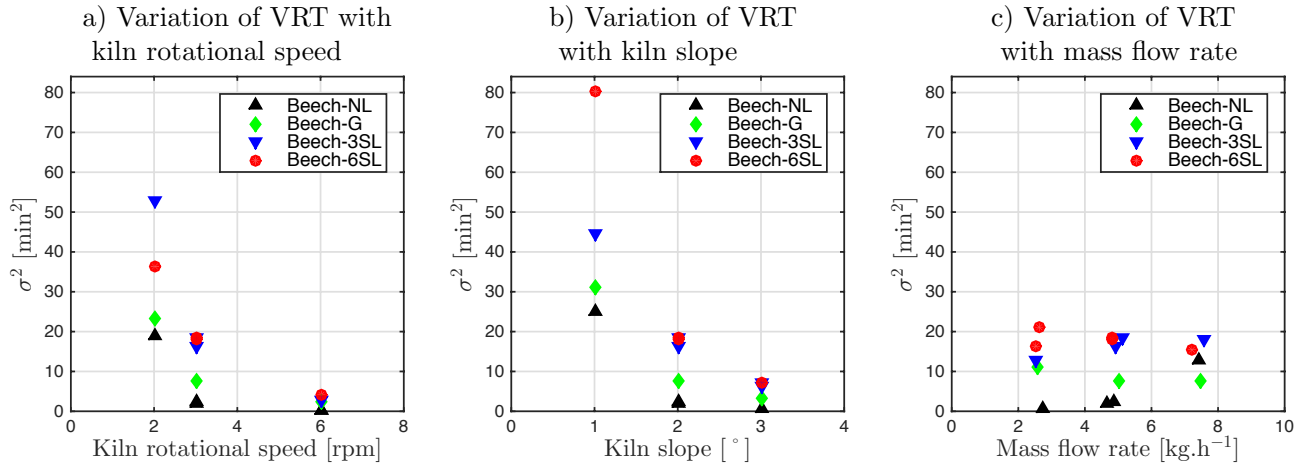

(c) Variance of residence time.

Fig. 6: Influence of operating parameters (N, S and $\dot{M}$) on the MRT, HU[%] and VRT, for the flow of beech chips, when the kiln is equipped without lifters, with a grid, or with 3 and 6 rows of straight lifters.

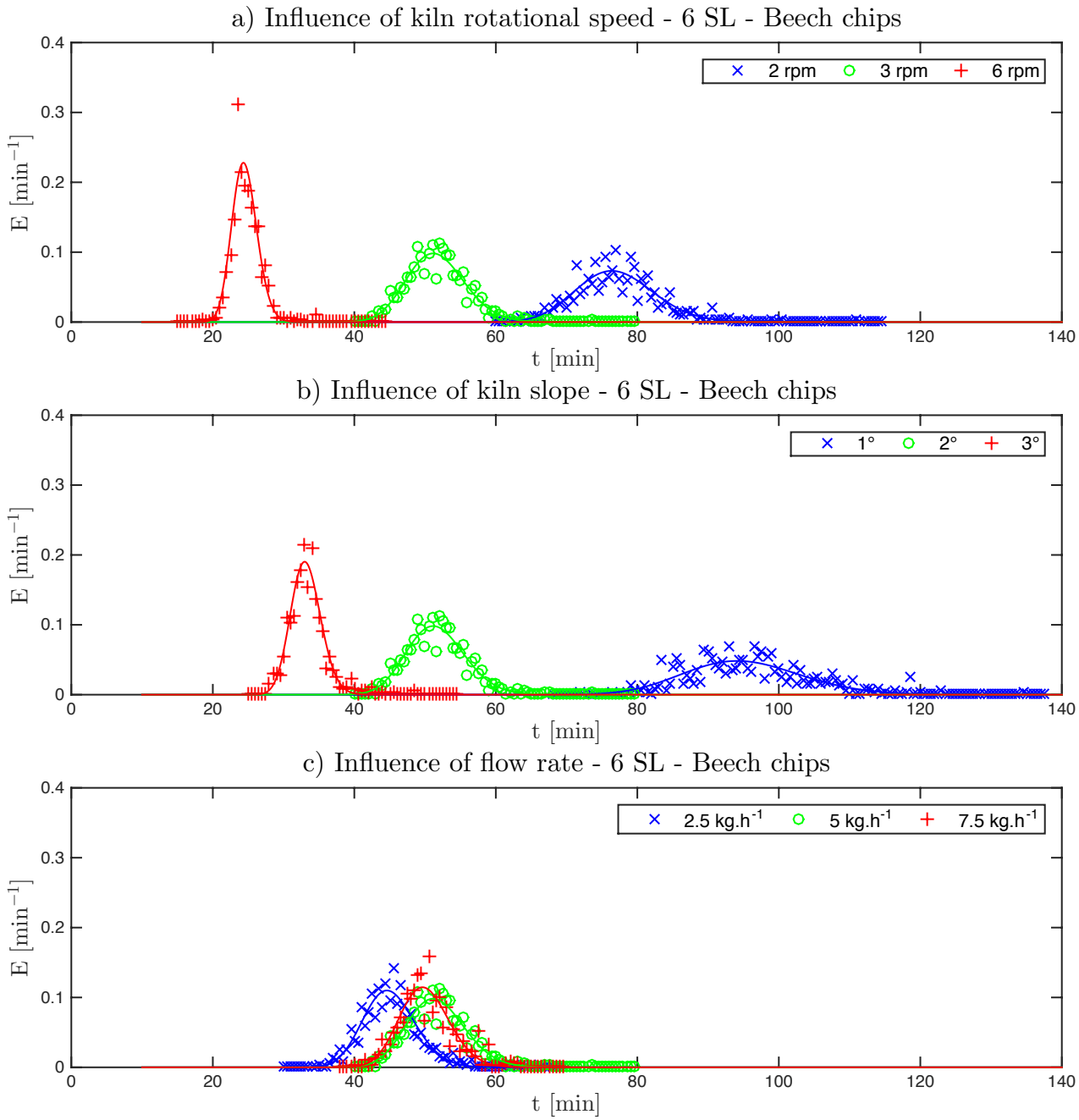

Fig. 7: Influence of operating parameters (N, S and $\dot{M}$) on the RTD for the flow of beech chips, when the kiln is equipped with 6 rows of straight lifters. Solid lines represent the axial dispersion model using fitted parameters.

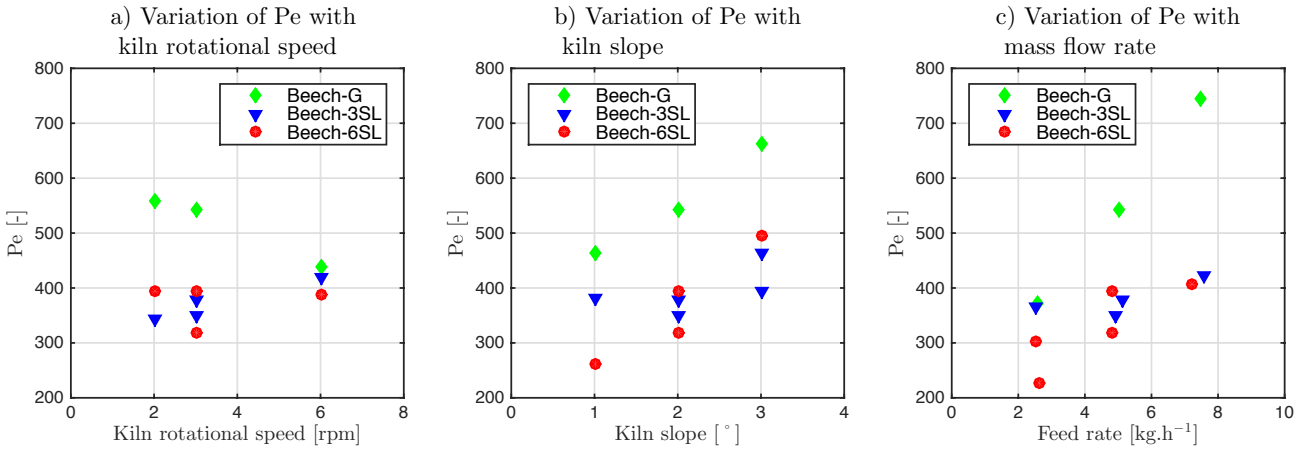

(a) Peclet number.

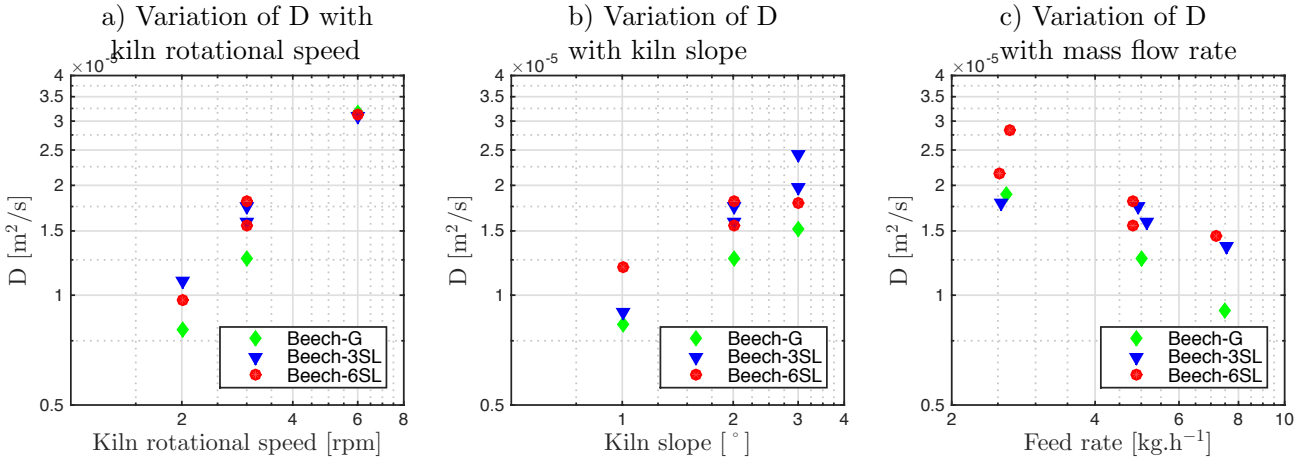

(b) Axial dispersion coefficient.

Fig. 8: Influence of operating parameters (N, S and $\dot{M}$) on the Pe and D, for the flow of beech chips, when the kiln is equipped with a grid, or with 3 and 6 rows of straight lifters.

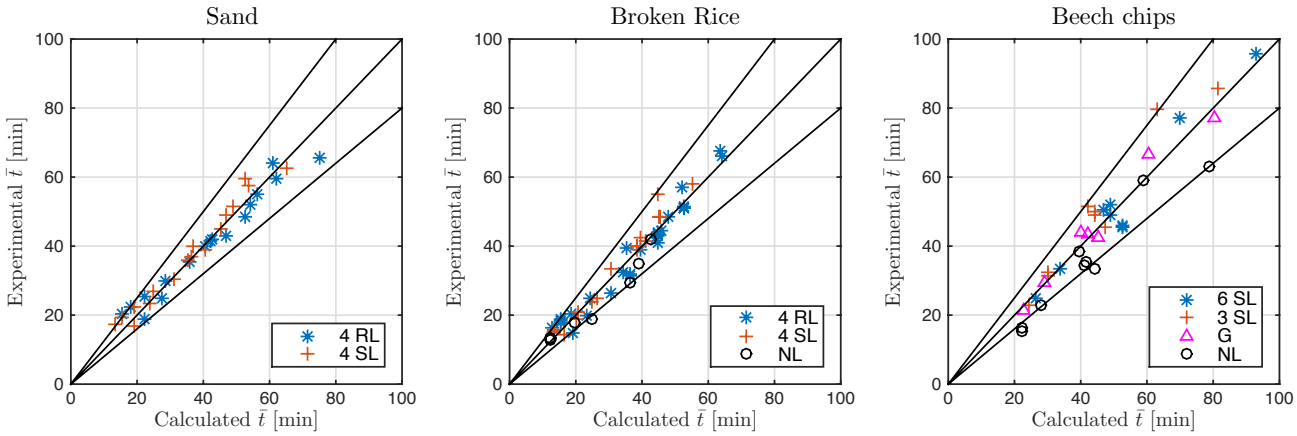

(a) Mean Residence time.

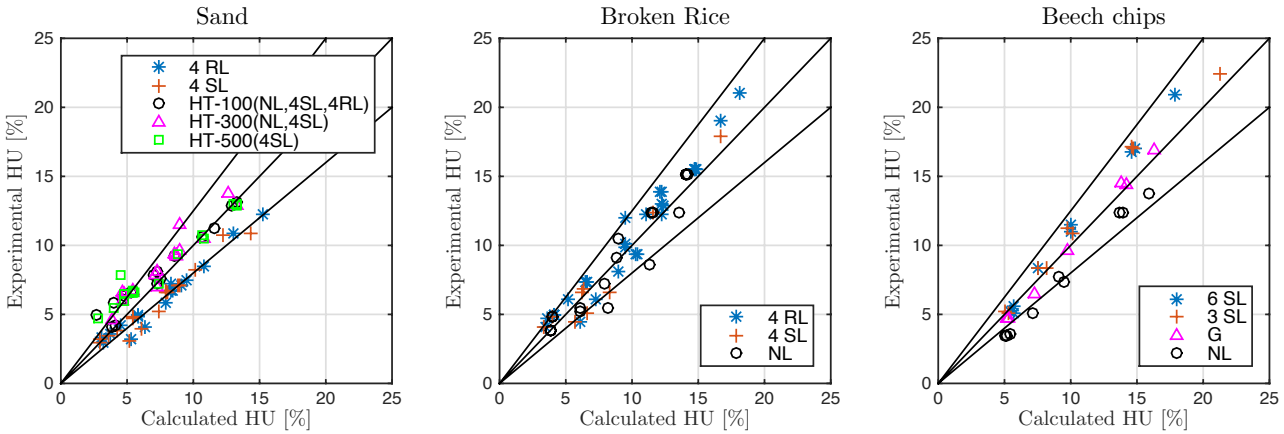

(b) Fractional volumetric hold up (filling degree).

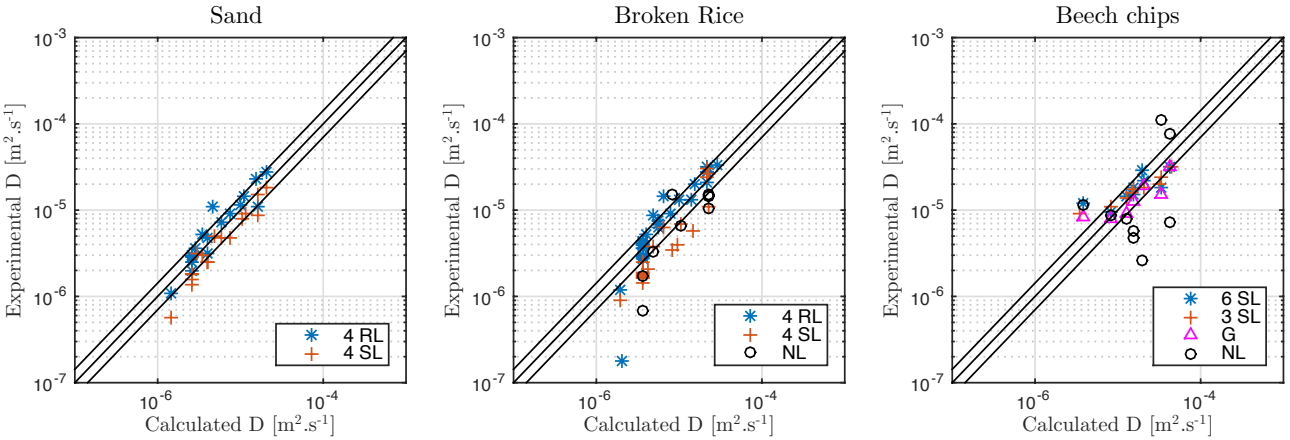

(c) Axial dispersion coefficient.

Fig. 9: Comparison of the experimental MRT, HU[%] and D, while using sand (left), broken rice (middle), and beech chips (right), with the calculated values from Eq.9 using the sets of parameters given in Table 3. Solid lines are ±20% margins.

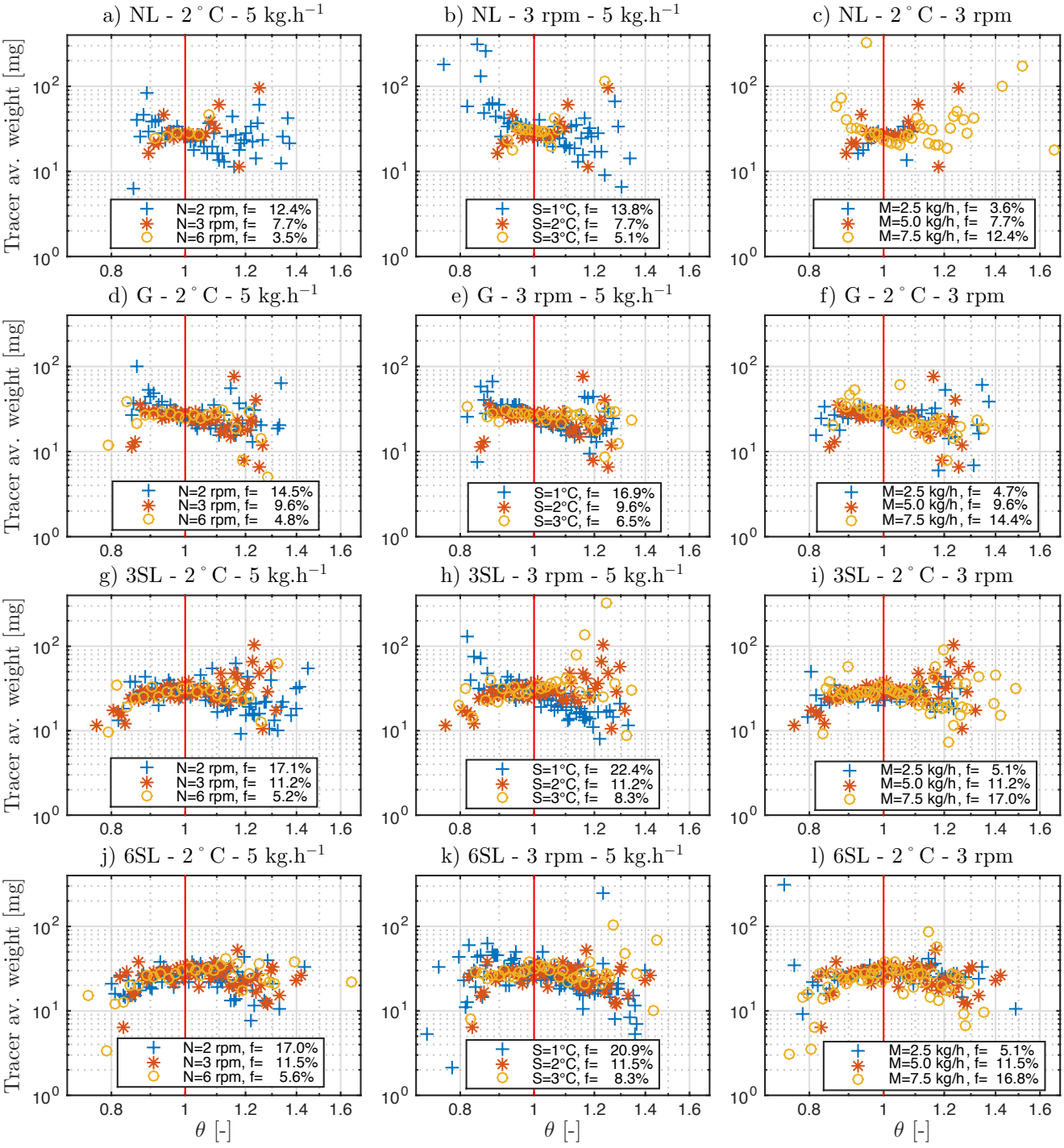

Fig. 10: Influence of operating parameters N (a-d-g-j), S (b-e-h-k) and $\dot{M}$ (c-f-i-l) on the tracer average weight (function of dimensionless time) for the flow of beech chips, when the kiln is equipped with: NL (1st row), G (2nd row), 3SL (3rd row) and 6SL (4th row). The dimensionless time is defined as $\theta = t/\bar{t}$ and so the red lines represent the time when $t = \bar{t}$.

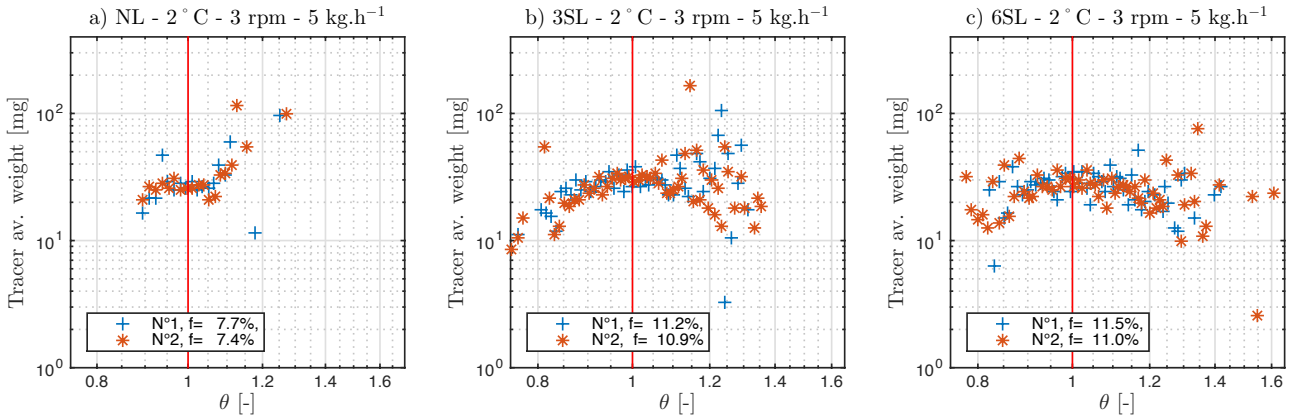

Fig. 11: Reproducibility of segregation of beech chips when the kiln is operated within the defined benchmark value for the operating parameter, and equipped with 3 or 6 rows of straight lifters or without lifters.

7. Tables

Table 1: Geometrical characteristics of the rotary kiln and order of magnitude of operating conditions achieved in this study.

Subsets	Parameters	Order of magnitude	Remarks
Rotary kiln	D_i[m]	0.21	Internal diameter
	L [m]	4.20	Kiln length
Operating conditions	N [rpm]	2-6	Rotational speed
	S [°]	1-3	Kiln slope
	$\dot{M}$ [kg.h^{-1}]	2.5-7.5	Mass flow rate
	Lifters shape	None	Smooth wall
	and	Grid (16 rows)	5 mm height
	configurations	3 SL, 6SL	30 mm height

Table 2: Physical properties of granular materials.

Product	Shape	ρ_{true} [kg.m^{-3}]	ρ_{bulk} [kg.m^{-3}]	ρ_{tapped} [kg.m^{-3}]	Size [mm]	θ [°]
Beech chips	Parallelepiped	1506	260	284	10×4.5×2	42
Beech chips tracer	Parallelepiped	-	279	310	10×4.5×2	42

Table 3: Determined parameters for the models proposed for the mean residence time, the filling degree and the axial dispersion, with associated confidence intervals.

Model	$\bar{t}$	Confid. interval		HU[%]	Confid. interval		D	Confid. interval	
parameters	Value	Inf.	Sup.	Value	Inf.	Sup.	Value	Inf.	Sup.
k	**0.0026**	-0.0023	0.0074	**45.65**	5.74	85.56	$\mathbf{1.52\,10^{-4}}$	$-8.92\,10^{-4}$	0.0012
α	**-0.4422**	-0.5367	-0.3478	**-0.4439**	-0.5506	-0.3372	**0.7483**	0.3033	1.1933
β	**-0.3597**	-0.4715	-0.2478	**-0.3987**	-0.5229	-0.2745	**0.2996**	-0.1362	0.7354
γ	**0.9276**	0.7730	1.0822	**0.7780**	0.6296	0.9263	**1.9859**	0.6477	3.3240
δ	**-0.1130**	-0.1574	-0.0686	**0.9584**	0.7814	1.1354	**-0.4511**	-1.2280	0.3259
ϵ	**-8.8835**	-11.459	-6.3081	**-3.8197**	-6.5517	-1.0878	**1.2185**	-13.809	16.246
ζ	**-2.4641**	-5.3569	0.4286	**16.763**	14.275	19.252	**5.5513**	-4.7868	18.889
η	**1.1**[13]	NA	NA	**0**	-	-	**0**	-	-

Table 4: Reproducibility of experiments: experimental hold-up, mean residence time, variance of residence time, Peclet number and axial dispersion.

Operating	HU	[kg]	$\bar{t}$	[min]	σ^2	[min²]	Pe	[-]	D	[m^2/s]
conditions	Values	$\frac{\Delta HU}{HU}$ [%]	Values	$\frac{\Delta \bar{t}}{\bar{t}}$[%]	Values	$\frac{\Delta \sigma^2}{\sigma^2}$[%]	Values	$\frac{\Delta Pe}{Pe}$[%]	Values	$\frac{\Delta D}{D}$[%]
3 rpm, 2°,	2.920	±4.47	35.20	±1.51	1.81	±25.51	1370	±28.38	0.0610	±29.86
5 kg.h^{-1}, NL	2.785		34.64		2.38		1013		0.0838	
3 rpm, 2°,	4.235	±2.95	49.06	±1.48	16.42	±11.28	297.2	±8.21	0.2016	±6.73
5 kg.h^{-1}, 3SL	4.105		49.84		18.50		272.5		0.2165	
3 rpm, 2°,	4.345	±4.45	51.78	±5.57	18.19	±1.38	298.7	±12.33	0.1901	±17.86
5 kg.h^{-1}, 6SL	4.145		48.81		18.46		262.1		0.2298	

Table 5: Results of the experimental matrix set for the RTD measurements.

Operating conditions			NL					Grid					3SL					6SL				
N	S	$\dot{M}$	HU	$\bar{t}$	σ^2	Pe	D	HU	$\bar{t}$	σ^2	Pe	D	HU	$\bar{t}$	σ^2	Pe	D	HU	$\bar{t}$	σ^2	Pe	D
[rpm]	[°]	[kg.h^{-1}]	[kg]	[min]	[min²]	[-]	[m^2/s]	[kg]	[min]	[min²]	[-]	[m^2/s]	[kg]	[min]	[min²]	[-]	[m^2/s]	[kg]	[min]	[min²]	[-]	[m^2/s]
3	**2**	**5**	2.920	35.20	1.81	1728	0.0484	3.615	43.54	7.49	541.4	0.1258	4.235	49.06	16.42	349.6	0.1745	4.345	51.78	18.19	318.3	0.1801
3	**2**	**5**	2.785	34.64	2.38	1467	0.0582	-	-	-	-	-	4.105	49.84	18.50	377.8	0.1591	4.145	48.81	18.46	394	0.1549
2	2	5	4.690	59.07	18.77	590	0.0853	5.490	66.52	23.30	557.5	0.0805	6.470	79.56	52.91	344.8	0.1095	6.440	77.26	36.48	394.3	0.0974
6	2	5	1.310	15.34	0.18	2629	0.0728	1.805	21.47	2.19	437.5	0.315	1.985	22.71	2.70	418.8	0.3109	2.135	24.76	4.21	387.5	0.3111
6	2	5	1.310	16.38	0.16	233.1	0.7721	-	-	-	-	-	-	-	-	-	-	-	-	-	-	-
3	**1**	5	5.215	62.95	25.12	416.4	0.1126	6.390	76.98	31.29	463.5	0.0833	8.470	85.61	44.78	382.7	0.0902	7.905	95.98	80.40	260.8	0.1193
3	**3**	5	1.940	23.00	0.51	114.8	0.1126	2.450	29.42	3.47	662	0.1525	3.150	31.33	6.34	393.1	0.3426	3.150	33.40	7.35	495.9	0.1794
3	**3**	5	-	-	-	-	-	-	-	-	-	-	-	32.50	7.14	464.8	0.1970	-	-	-	-	-
3	2	**2.5**	1.375	33.54	0.68	3392	0.0259	1.760	42.34	11.31	373	0.1882	1.935	45.29	12.75	365.3	0.1787	1.930	45.81	21.11	228.2	0.2842
3	2	**2.5**	-	-	-	-	-	-	-	-	-	-	-	-	-	-	-	1.950	45.26	16.53	303.7	0.2163
3	2	**7.5**	4.675	38.53	12.96	996.8	0.0785	5.450	43.73	7.46	746.3	0.0912	6.425	51.73	18.25	422.4	0.1363	6.340	50.37	15.42	407.5	0.145